Resonant photo-pumping x-ray-laser scheme using intense characteristic x rays for water-window radiation generation

Tetsuya Kawachi[1,*] and Yoshiaki Kato[2]

[1]*Quantum Beam Science Directorate, Japan Atomic Energy Agency (JAEA) 8-1-7, Umemidai, Kizugawa, Kyoto 619-0215, Japan*

[2]*The Graduate School for the Creation of New Photonics Industries 1955-1, Kurematsu, Hamamatsu, Shizuoka 431-1202, Japan*

(Received 26 August 2011; published 28 December 2011)

A line pair for a resonant photo-pumping x-ray-laser scheme is proposed in which the wavelength matching between the aluminum $K\alpha_2$ line ($\lambda = 0.833\ 95$ nm) and the $2p^6$-$(2p_{1/2},4d_{3/2})_1$ transition of the neonlike zinc ions ($\lambda = 0.834\ 00$ nm) is used. The population kinetics code of the neonlike zinc ions in plasma under irradiation of the aluminum $K\alpha$ line shows that substantial amplification gain can be generated in the transition of $(2p_{1/2},3p_{1/2})_0$-$(2p_{1/2},4d_{3/2})_1$ at a wavelength of 3.5 nm. We also investigate the experimental arrangement of this scheme, which implies that this scheme is feasible with the present ultra-short-pulse-laser technology.

DOI: 10.1103/PhysRevA.84.063848 PACS number(s): 42.55.Vc, 52.20.−j, 42.60.By

I. INTRODUCTION

Due to advances in x-ray-laser (XRL) physics and high-power-laser technologies, laboratory-size laser-driven plasma XRLs have been realized with the transient collisional excitation (TCE) scheme [1–3]. With the TCE scheme, highly coherent ultra-short-pulse soft XRLs are available in the wavelength region of 10–30 nm by pumping with Ti:sapphire lasers with 1-J energy and 10-Hz repetition rates [4]. At the shorter wavelength region, however, the wavelength of the TCE XRL has been limited to 7.3 nm where several tens of joules of laser energy were required for pumping to achieve intense lasing [5]. Since the extension of the lasing to shorter wavelengths, especially in the water-window region ($\lambda =$ 2.33–4.37 nm), will enable us to expand the applications of laboratory-size coherent x-ray sources to biological science [6], it will be very important to investigate alternative XRL schemes toward the shorter wavelength region.

One of the candidates of the water-window XRL is the photo-pumping XRL where several schemes have been investigated theoretically [7–10]. Resonant photo-pumping is one of them in which a spectral line emission from particular ions is absorbed by different element ions to create the population inversion in the latter. The success of this scheme as an XRL depends upon exact spectral matching between the emission line and the absorption line. Spectroscopic studies of highly charged ions in laser-produced plasmas were performed to find the line pairs suitable for the resonant photo-pumping scheme [11–14]. Also, the accurate wavelengths of many spectral lines of highly charged ions were determined by use of the electron-beam ion trap (EBIT). The data obtained by the EBIT group were used to find the candidate pairs of ions for photo-pumping XRLs [7].

Several experimental attempts have been made to test the resonantly photo-pumped XRL by using plasmas composed of highly charged ions for the emitter and for the absorber [15–19]. At Lawrence Livermore National Laboratory, the SHIVA and NOVETT laser facilities were used to design the x-ray flash lamps for several resonant photo-pumping schemes [15,16]. At Sandia National Laboratory [17], a Saturn Z-pinch machine was used to test the heliumlike sodium $1s$-$4p$ laser pumped by the resonance line of heliumlike neon ions, which was the scheme proposed by Vinogradov *et al.* [20]. The kryptonlike molybdenum (Mo VII) ion laser pumped by galliumlike molybdenum ions (Mo XII), proposed by Feldman *et al.* [21], was investigated at Princeton University [18]. Despite these intensive investigations, significant amplification has not been observed in the resonant photo-pumping scheme. This indicates the difficulty of using highly charged ions for both the emitter and the absorber.

Although the resonant photo-pumping is straightforward in its concept, several technical difficulties have to be overcome for realization of this scheme. For example, the emitter and the absorber ions should be located as close as possible so that the pumping emission reaches the absorber ions efficiently. At the same time, the electron temperature of the emitter should be high to increase the emissivity of the pumping radiation, whereas, a lower temperature is preferred for the absorber ions to avoid the thermal population in the lower lasing level. Satisfying these two conditions simultaneously is necessary in this scheme.

Another photo-pumping scheme is the photo-ionization scheme or continuum x-ray pumping scheme in which population inversion is obtained with the inner-shell ionized atoms that are generated by pumping with ultrafast x rays [8–10]. The photo-ionization schemes based on the proposal by Duguary and Rentzepis [22] have been tested by use of the Z-pinch plasma or the laser-produced plasmas [16], [23–25]. However, significant gain has not been obtained in the x-ray region. In this scheme, the generation rate of the population inversion competes with other atomic processes, such as autoionization and electron-impact collisional ionization of the gain medium ions, leading to quite short gain durations of only a few femtoseconds. The success of this scheme depends on the development of an intense ultrafast pumping x-ray source and very precise traveling-wave pumping. Recently, the atomic inner-shell XRL pumped by intense short-duration x-ray radiation from an x-ray-free-electron laser (X-FEL) was proposed [26]. Although X-FEL almost is an ideal source for pumping the inner-shell ionization XRLs, we note that X-FEL might not be suitable as the pumping source for the resonant photo-pumping scheme due to the broad bandwidth of the X-FELs at present.

*kawachi.tetsuya@jaea.go.jp

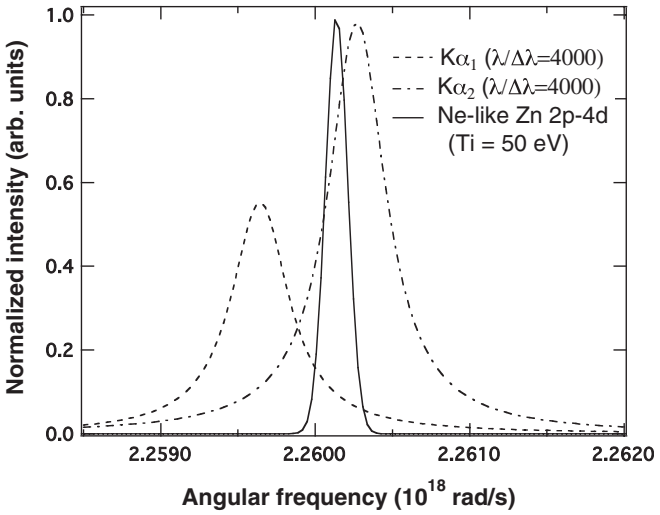

FIG. 1. Comparison of spectral profiles of the aluminum $K\alpha_1$ and $K\alpha_2$ lines and the $2p^6$-$2p^5 4d$ resonance line of the neonlike zinc ion.

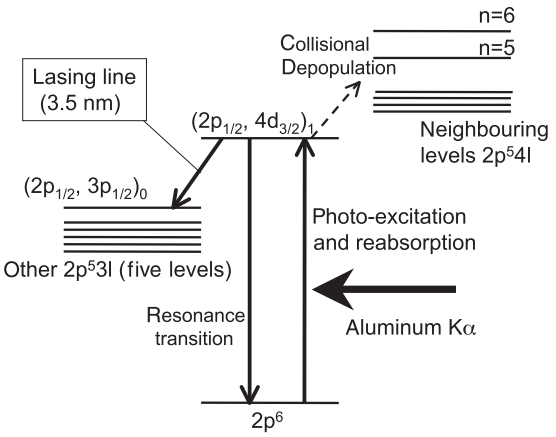

FIG. 2. Simplified energy-level diagram of the neonlike zinc ions. The aluminum $K\alpha$ photons can be absorbed by the transition of the $2p^6$-$2p^5 4d$ $(2p_{1/2},4d_{3/2})_1$.

It is noted that the photo-pumping processes are quite attractive in terms of the recent progress of X-FELs and laboratory astrophysics. For the X-FELs [27–29], the photo-pumping XRLs are of interest as the x-ray seeder in the water-window and other wavelength regions, which significantly improves the temporal coherence of the X-FEL compared with that in the self-amplified spontaneous emission mode. In laboratory astrophysics, the photo-absorption process in the x-ray region in plasmas has received attention as an opacity project [30] and, more recently, as photo-excited plasmas [31]. Therefore, the study of the population kinetics of the photo-pumped plasmas will contribute to a deeper understanding of the plasma processes in astrophysics.

In this paper, we investigate the feasibility of the resonant photo-pumping XRL scheme using $K\alpha$ emission from a solid target as the pumping source. The advantage of $K\alpha$ emission as the pumping source is that emissions of other photons are weak in the plasma in which $K\alpha$ photons are efficiently emitted. We note that efficient generation of the subpicosecond duration $K\alpha$ pulse has been demonstrated, and the energy conversion efficiency from the pumping laser to $K\alpha$ emission reaches $\sim 10^{-4}$/sr [32,33]. Furthermore, since $K\alpha$ photons are emitted in a localized area quite close to the solid surface, the distance from the location of $K\alpha$ emission to the absorption medium can be kept short, making the $K\alpha$ source advantageous in terms of the pumping efficiency.

We take the wavelength matching of the aluminum $K\alpha_2$ line (0.833 95 nm) and the $2p^6$-$(2p_{1/2},4d_{3/2})_1$ resonance line of the neonlike zinc ions (0.834 00 nm) as an example. Although the use of the neonlike ions as the gain medium ions has already been proposed in Ref. [7], the use of $K\alpha$ radiation as the pump source was not. Figure 1 shows the line profiles of the $K\alpha_1$, the $K\alpha_2$, and the $2p^6$-$(2p_{1/2},4d_{3/2})_1$ resonance lines of the neonlike zinc ions. The wavelengths of these lines have been investigated well theoretically and experimentally [34–37]. The substantial overlap of the $K\alpha_2$ and the resonance lines indicates that strong photo-absorption can be expected.

Figure 2 shows the simplified energy-level diagram of the neonlike zinc ions. Due to the photo-excitation of the $2p^6$-$(2p_{1/2},4d_{3/2})_1$ transition, population inversion between the $(2p_{1/2},4d_{3/2})_1$ and the $(2p_{1/2},3p_{1/2})_0$ levels is expected. The use of neonlike ions has two advantages: The first is that the neonlike ions are a stable ionic species and have large ion abundances in plasmas. The second is that, because the $(2p_{1/2},4d_{3/2})_1$ level is not an autoionization level, the lifetime of the upper lasing level is a few tens of femtoseconds. Since this lifetime, which is determined mainly by the radiative transition probability, is much longer than that in the inner-shell ionization scheme (a few femtoseconds), we do not need to employ ultra-short-pulse and precise traveling-wave pumpings in the present case.

In the following, we present theoretical calculations of the photo-absorption of the $K\alpha$ line in the neonlike zinc plasmas under given plasma conditions and investigate the feasibility of this scheme as an XRL medium.

II. THEORETICAL MODEL

In our calculation model, 13 excited levels in total are included (see Fig. 2). For the excited levels of $2p^5 nl$ with $n = 3$, we include six levels, i.e., $(2p_{1/2},3s_{1/2})_1$, $(2p_{3/2},3s_{1/2})_1$, $(2p_{1/2},3p_{1/2})_0$, $(2p_{1/2},3p_{3/2})_1$, $(2p_{1/2},3d_{3/2})_1$, and $(2p_{1/2},3d_{5/2})_2$ levels. For the excited levels of $2p^5 nl$ with $n = 4$, the level energies of the $2p^5 4s$, $2p^5 4p$, and $2p^5 4f$ levels are averaged over their fine-structure levels, and for the $2p^5 4d$ levels, the $(2p_{1/2},4d_{1/2})_1$ and $(2p_{1/2},4d_{3/2})_1$ levels are treated separately. The energies of these levels are referred from the HULLAC code [38], and especially for the $(2p_{1/2},3p_{1/2})_0$ and $(2p_{1/2},4d_{3/2})_1$ levels, we use the atomic data presented by the National Institute of Standards and Technology (NIST) [34] and the experimental investigation by Kallne and Aberg [35]. For higher-lying levels of $2p^5 n$ ($n = 5$ and 6), we assume hydrogenic approximation with an effective nuclear charge of $z_{\rm eff} = 20$. In the following context, we denote the $(2p_{1/2},3p_{1/2})_0$ and $(2p_{1/2},4d_{3/2})_1$ levels as $2p^5 3p$ and $2p^5 4d$, respectively.

Atomic processes included in the calculation are the spontaneous emission, the electron-impact excitation and deexcitation, the electron-impact ionization, and the radiation-trapping effect of the $2p^6$-$2p^5 4d$ resonance line. The

spontaneous emission probability and the electron-impact excitation cross section are calculated by use of the HULLAC code, and the electron-impact ionization cross section from the ground state and the excited levels is derived by the scaled hydrogenic approximation [39]. The rate coefficients of the excitation and the ionization are derived under the assumption of the Maxwellian electron-velocity distribution. The electron-impact deexcitation rate coefficients are estimated from the excitation rate coefficient by use of the principle of detailed balance. The plasma is assumed to be in the ionizing phase, i.e., we ignore the recombination processes.

The size of the zinc plasma is assumed to be 20 μm $\times$ 20 μm $\times$ 5 mm in the x, y, and z directions, respectively, as shown in Fig. 3 where z is along the length of the gain region. We divide the plasma into thin-sliced areas with sizes of 20 μm $\times$ 20 μm $\times$ 100 nm. Each sliced area is divided into 100 $\times$ 100 cells with sizes of 200 $\times$ 200 nm in the x-y plane. The plasma parameters of this sliced area are assumed to be $T_e = 200$ eV, $n_e = 2 \times 10^{21}$ cm^{-3}, $T_i = 50$ eV, and $n_{\text{nelike}} = 1 \times 10^{20}$ cm^{-3}, where T_e is the electron temperature, n_e is the electron density, n_{nelike} is the neonlike ion density, and T_i is the ion temperature. The validity of these values is described later. Under the present plasma parameters, each cell includes 4×10^5 ions. The $K\alpha_2$ photons come into the sliced area from the y direction. The line profile of the $K\alpha_{1,2}$ lines is assumed to be Lorentzian with a linewidth ($\Delta\lambda/\lambda$) of $\sim 2.5 \times 10^{-4}$ [40], and the line profile of the $2p^6$-$2p^5 4d$ resonance line is Gaussian with the Doppler broadening corresponding to the ion temperature T_i as shown in Fig. 1. In Ref. [37], it is reported that the linewidth of the $2p^6$-$2p^5 4d$ resonance line is broader than the present assumption, which implies that the photo-absorption may be more substantial than the present calculation. In the following, we denote $K\alpha_2$ as $K\alpha$ unless specifically stated.

The ion that absorbs a $K\alpha$ photon reemits a photon corresponding to the $2p^6$-$2p^5 4d$ resonance transition with a lifetime of 23 fs, and this emitted photon may be absorbed by another ion. In the present calculation, we take the radiation transport in the x-y plane into account. The radiation transport in the z direction is ignored because the number of photons of the resonance line coming into the calculation area from the neighboring sliced area is balanced with those going out of the calculation area to the neighboring sliced area.

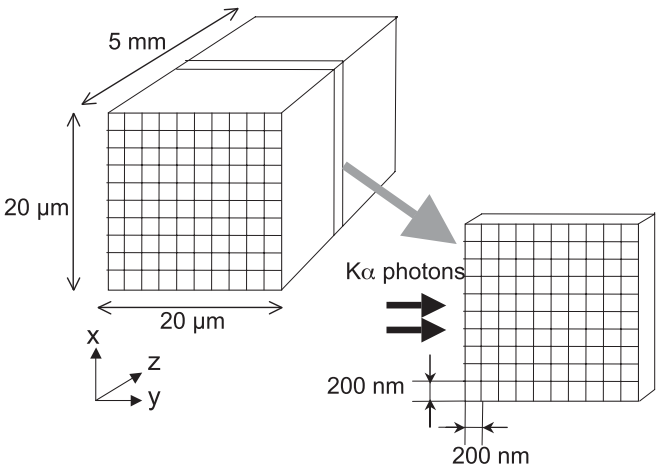

FIG. 3. Schematic of the calculation area. The plasma with a size of 20 μm $\times$ 20 μm $\times$ 5 mm is divided into a sliced area with a thickness of 100 nm. Each sliced area is divided into cells with 200 $\times$ 200 nm in the x-y plane. $K\alpha$ photons are incident from the y direction into each sliced area.

The procedure to calculate the temporal evolution of the $2p^5 4d$- and $2p^5 3p$-level populations is as follows: First, the x position where the $K\alpha$ photon is incident into the sliced area and the angular frequency of the $K\alpha$ photon within the linewidth are determined randomly. Second, the y position of the ion that absorbs the $K\alpha$ photon is calculated according to the absorption probability derived from the absorption length of the $K\alpha$ photon in the plasma. If the y value is larger than 20 μm, the $K\alpha$ photon passes through the plasma. If the y value is smaller than 20 μm, we record the x and y values as the position of the $2p^5 4d$ ion. This routine is repeated N times, where N is the number of $K\alpha$ photons coming into the calculation area in a time step $\Delta t = 1$ fs. It is noted that the time step of 1 fs is sufficiently small since the spontaneous transition probability of the resonance line is $\sim$23 fs. For each $2p^5 4d$ ion in each cell, there are three cases: (1) The ion emits the resonance line, (2) other collisional-radiative population-depopulation processes take place, and (3) nothing happens under the time step of 1 fs. In the case ion which the ions emit photons, the frequency is determined randomly within the spectral linewidth, and the direction of the emission in the x-y plane is determined randomly. According to the absorption probability derived from the absorption length of the $2p^6$-$2p^5 4d$ resonance line, we determine whether the emitted photon is absorbed by another ion or escapes from the plasma. If the photon is absorbed in the plasma, the *old* (x,y) position is replaced by the *new* one.

In the case in which the collisional-radiative depopulation occurs, the $2p^5 4d$ ion in the (x,y) position is annihilated. We also include the population process from other levels into the $2p^5 4d$ level where the initial populations of the other levels are derived from the quasi-steady-state approximation under the given T_e and n_e. The above procedure is iterated for all the $2p^5 4d$ ions in the sliced area by including additional incident $K\alpha$ photons with the temporal envelope.

III. CALCULATED RESULTS AND DISCUSSION

At first, we consider the case in which 1×10^6 $K\alpha$ photons come into each sliced area at $t = 0$ fs and no $K\alpha$ photons come after that. Figure 4 shows the spatial distribution of the $2p^5 4d$ excited-level populations at $t = 1$, 100, and 500 fs where the ordinate is normalized by the total number of $2p^5 4d$ ions in the sliced area. The calculated result shows that around 18% of the $K\alpha$ photons are absorbed in the plasma, and they are absorbed mainly in the region of $y = 0$–10 μm. Hereafter, we call the regions of $y = 0$–2 and 2–10 μm the *edge* region and the *internal* region, respectively. For the *internal* region of the plasma, the population of the $2p^5 4d$ level decreases slower than that of the *edge* region. This is because, under the present plasma parameters with a $K\alpha$ absorption length of 200 nm, the resonance emission in the *edge* region easily escapes from the plasma, whereas, the emission in the *internal* region of the plasma is re-absorbed by the neighboring ions. Figure 5 shows the temporal evolution of the $2p^5 4d$-level population

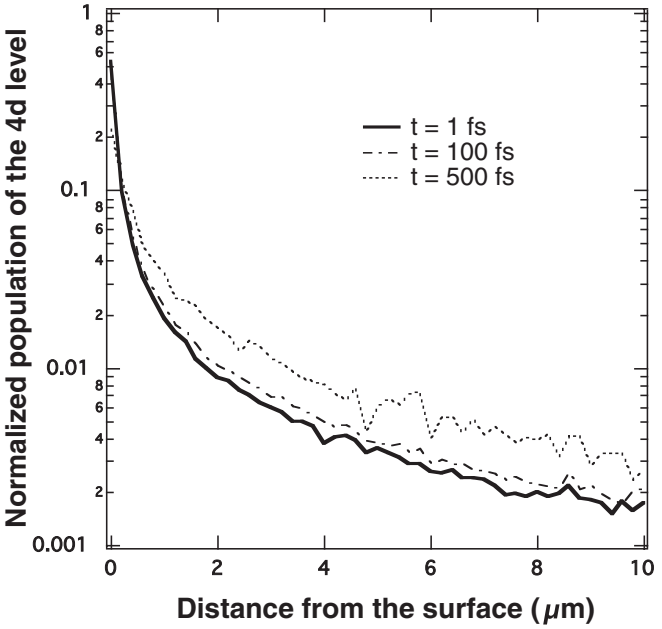

FIG. 4. The temporal evolution of the normalized $2p^5 4d$ population under the condition that 1×10^6 photons come into each sliced area in 1 fs. Due to the radiation-trapping effect, the decay constant becomes larger as the distance from the surface becomes long.

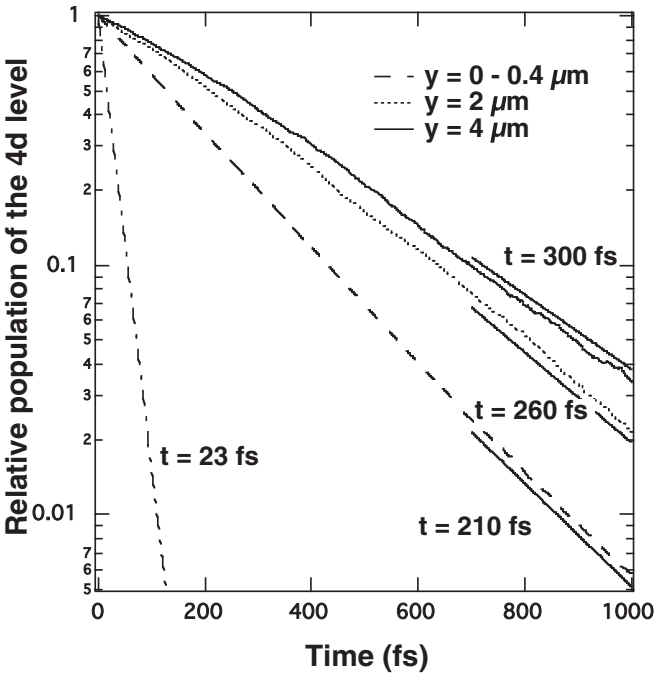

FIG. 5. The temporal evolution of normalized $2p^5 4d$-level populations for various y positions from the surface. The solid-dotted line indicates the natural lifetime of the $2p^5 4d$ level (23 fs). At the *internal* region of the plasma (i.e., $y = 4$ μm), the lifetime is longer than that at the *edge* region ($y = 0$–0.4 μm). In $t = 0$–400 fs, the decays are slower than those at a later time for $y = 2$ and 4 μm due to the photo-pumping effect from the *edge* region.

for various y positions. The solid line, the dotted line, and the hatched line correspond to the positions of $y = 0$–0.4, 2, and 4 μm, respectively. With the solid-dotted line, we show the decay of the $2p^5 4d$ level corresponding to the lifetime of the resonance line (23 fs) as a reference. The calculated result shows that, even in the *edge* region, the radiation-trapping effect takes place since the effective lifetime of 210 fs is longer than the natural lifetime by a factor of ∼9. This effect is more obvious in the *internal* region ($y \sim 4$ μm); the decay constant reaches ∼300 fs. This long lifetime becomes advantageous for the XRL. It should be noted that, in the early time region of $t < 400$ fs, there is a small hump for the case of $y = 2$ and 4 μm, and the slopes of the dotted and solid lines (or effective lifetime) are slower than the slopes at the later time region ($t > 700$ fs). This is due to the photo-pumping effect by the emission from the *edge* region where the $2p^5 4d$ population is much larger than that in the *internal* region.

Next, we assume that the pumping $K\alpha$ pulse has a Gaussian temporal profile with a duration of 500-fs full width at half maximum (FWHM). The total photon number is assumed to be 5×10^{11} or 50 μJ in the energy, which corresponds to 1×10^8 $K\alpha$ photons coming into each sliced area. As the initial condition, we assume that all excited-level populations are described by the collisional-radiative equilibrium under the plasma parameters with $T_e = 200$ eV, $n_e = 2 \times 10^{21}$ cm^{-3}, and $n_i = 1 \times 10^{20}$ cm^{-3}. It is noted that, under these plasma parameters, the thermal populations of the excited levels are negligibly small. Figure 6 shows the temporal evolution of the $2p^5 3p$ and $2p^5 4d$ excited-level populations. The right-hand-side ordinate is $n(nl)/g(nl)$ averaged over the region of $y = 1$–5 μm where $n(nl)$ and $g(nl)$ are the excited-level population and the statistical weight of level nl, respectively. The corresponding amplification gain in the transition of $2p^5 3p$-$2p^5 4d$ at a wavelength of 3.5 nm is shown by the thick solid curve where the gain is given in cm^{-1} on the left-hand side. In this calculation, the intrinsic linewidth of the lasing line has been assumed to be Gaussian with the ion temperature $T_i = 50$ eV. The temporal profile of the pumping pulse (the intensity peak is at 500 fs) also is shown.

$n(4d)/g(4d)$ gradually increases as the pumping rate becomes large. The peak is obtained at around 600 fs, that is, slightly after the peak of the pumping pulse. This is because the depopulation from the $2p^5 4d$ level to the other levels, e.g., $2p^5 3p$, $2p^5 4p$, $2p^5 4f$, and $n = 5$ and 6 levels, becomes larger than the pumping rate by incident $K\alpha$ photons. Since the $2p^5 3p$ level mainly is populated due to the collisional depopulation and spontaneous transition from the $2p^5 4d$ level, the $2p^5 3p$-level population becomes maximum ∼200 fs after the peak of the $2p^5 4d$-level population. Amplification gain for the transition between the $2p^5 3p$ and the $2p^5 4d$ levels is generated for the time region of $t = 100$–900 fs, and the gain duration (FWHM) is about 500 fs. This duration is much longer than that expected in the continuum x-ray pumping schemes [8,9]. Therefore, the present scheme does not need precise traveling-wave pumping, which is one of the essential technical difficulties of the continuum x-ray pumping scheme. The peak value of the amplification gain is 110 cm^{-1}, which is sufficient for the substantial amplification for the plasma length of 5 mm.

We note that, in our model, the radiation-trapping effect of the $2p^6$-$2p^5 3s$ and $2p^6$-$2p^5 3d$ transitions has not been included. Because the $2p^5 3s$ and $2p^5 3d$ populations are

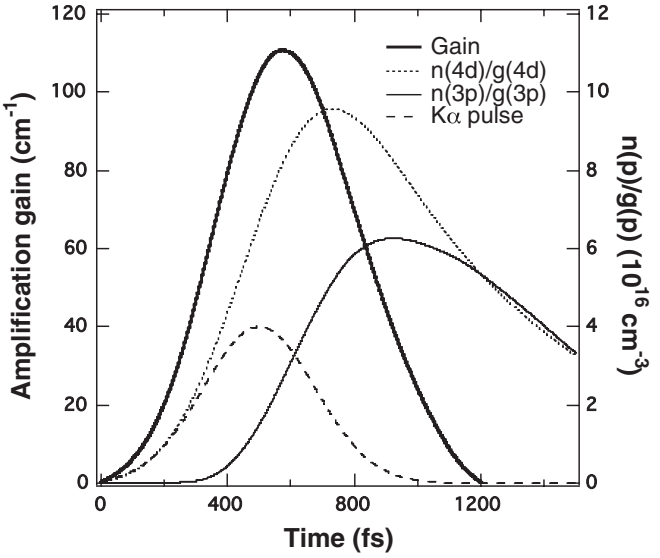

FIG. 6. The temporal evolution of the $2p^5 4d$ and $2p^5 3p$ excited-level populations divided by their statistical weights (dotted line and thin solid line). The amplification gain for the transition of the $2p^5 3p$-$2p^5 4d$ line also is shown (thick solid line). The envelope of the pumping $K\alpha$ line with a duration of 500 fs (FWHM) is shown by the dashed curve.

generated mainly from the $2p^5 3p$ level by the collisional processes, as long as the $2p^5 3p$ population is small, the $2p^5 3s$ and $2p^5 3d$ populations are small, and the radiation-trapping effect upon the $2p^5 3p$ population is not substantial. Indeed, under the assumption that spontaneous transition probabilities of the $2p^6$-$2p^5 3s$ and $2p^6$-$2p^5 3d$ transitions are set to be zero, the $2p^5 3p$ population slightly increases for the time region of $t > 600$ fs, and the decrease in the peak value of the amplification gain is only 5%.

It is valuable to estimate the saturation intensity for this scheme. The saturation intensity $I_{\rm sat}$, at the center of the frequency of the laser line, is determined by the depopulation rate of the upper and lower lasing levels and is expressed as

$$I_{\rm sat} = \frac{h\nu}{\sigma_{\rm se}\tau_2} = \frac{h\nu}{\frac{\lambda^2(\tau_1+\tau_2)}{4\pi^2 t_{\rm spont}}\tau_2}, \qquad (1)$$

where $h\nu$ is the photon energy of the XRL, $\sigma_{\rm se}$ is the stimulated emission cross section, τ_1 and τ_2 are the collisional-radiative depopulation times of the lower and upper lasing levels, respectively, λ is the wavelength of the lasing line, and $t_{\rm spont}$ is the decay time of the spontaneous transition of the lasing line. Under the present plasma parameters, the estimated saturation intensity is $I_{\rm sat} \sim 4 \times 10^{11}$ W/cm^2. As described later, this high-saturation intensity indicates the feasibility of the present photo-pumping XRL scheme as a useful laboratory-size coherent water-window soft x-ray source.

In Fig. 7, we present an example of the experimental setup of this scheme including the target and the pumping laser. The target is an aluminum foil of 4-μm thickness with a 0.2-μm-thick zinc coating. At first, the zinc side is irradiated with double pulses of a line-focused pumping laser ($\lambda = 1.053$ μm) with intensities of 10^{13} W/cm^2, separated by 100 ps. The length and width of the line focus are

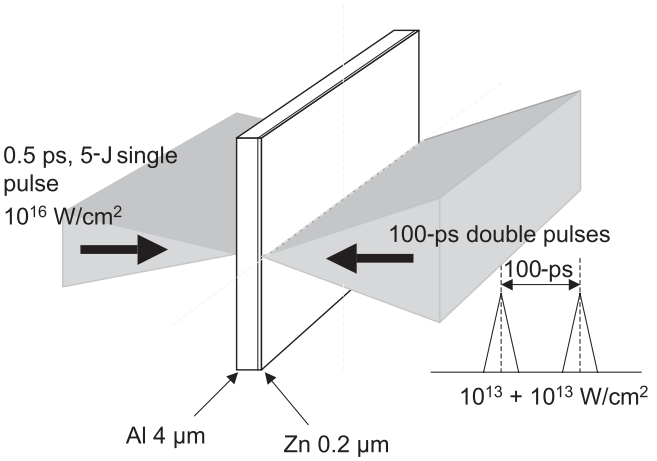

FIG. 7. Schematic of the setup of the photo-pumping scheme. The target consists of 4-μm-thick aluminum together with 0.2-μm zinc. The zinc side is irradiated by 100-ps-duration double pulses. After 100 ps from the peak of the second pulse, the opposite side is irradiated by an ultrashort pulse with 500-fs duration, 5 J, and 10^{16} W/cm^2 to generate an intense aluminum $K\alpha$ line.

assumed to be 5 mm and 50 μm, respectively. The role of this pumping laser is to prepare the neonlike zinc ions in plasma. The one-dimensional hydrodynamics simulation code HYADES [41] shows that, under the pumping-laser conditions, the appropriate aluminum and zinc plasmas can be prepared at $t_{\rm L} = 100$ ps as shown in Fig. 8 where $t_{\rm L}$ is measured from the peak of the second pulse. In Fig. 8, the aluminum plasma is located up to around $y = 0$–6 μm from the target surface, and the zinc plasma is located in $y > 6$ μm. The plasma parameters of $T_{\rm e} = 100$ eV, $n_{\rm e} = 2 \times 10^{21}$ cm^{-3}, $T_{\rm i} = 50$ eV, $n_{\rm nelike} = 1 \times 10^{20}$ cm^{-3} can be achieved in the

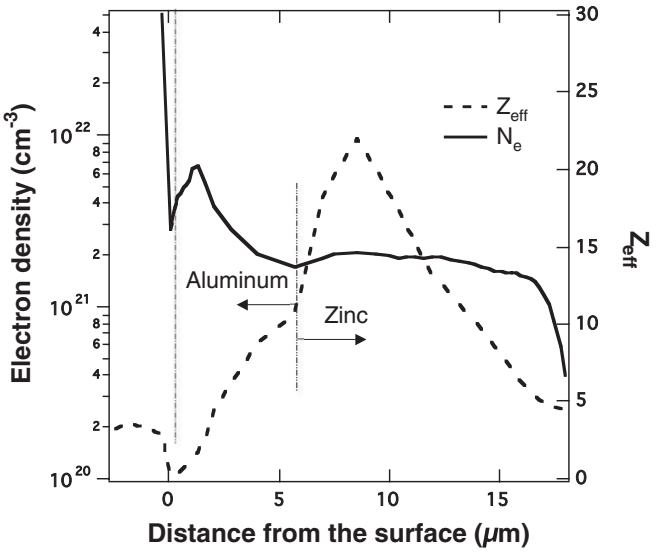

FIG. 8. Calculated result by the use of hydrodynamics simulation at 100 ps after the peak of the second pulse. The solid line is the electron density, and the dotted line is the effective nuclear charge. At $y = 6$–10 μm, the electron density and the effective nuclear charges of 15–22 are appropriate for the present XRL scheme with the neonlike Zn ions.

region of $y = 6$–12 μm. At this time, the aluminum side is irradiated by an ultrashort-laser pulse with traveling-wave pumping. We assume the duration is 500 fs (FWHM) and the intensity is 1×10^{16} W/cm^2. This intensity is optimum for the generation of aluminum $K\alpha$ photons [32]. With a line focus of 5-mm length and 20-μm width, the required pumping energy for the ultrashort optical pulse is only 5 J.

It is noted that the zinc ions generated in the opposite side of the $K\alpha$ generation may have expansion velocity in the y direction. However, the Doppler decoupling effect on the $K\alpha$ absorption by the resonance transition of $2p^6$-$2p^5 4d$ is not substantial because the hydrodynamics simulation shows that the velocity v, in the region of $y = 11$–16 μm from the target surface at $t = 300$ ps, is on the order of $v = 10^4$ m/s, i.e., $v/c \sim 3 \times 10^{-5}$, smaller by 1 order of magnitude than that of the linewidth of the $K\alpha$ line.

In terms of the energy conversion efficiency η, recent theoretical investigation shows $\eta \sim 10^{-4}$ per sr [33], and, at least, $\eta > 10^{-5}$/sr can be obtained in the expectation. Since the distance from the $K\alpha$ source (front side of the target) to the absorber ($y = 6$–12 μm) is around 10–16 μm with taking the thickness of aluminum into account, the effective solid angle of the $K\alpha$ source to the neonlike zinc plasma in the present geometry is around 3 sr. Therefore, we can deliver more than 100 μJ of $K\alpha$ photons into the zinc plasma where the transmittance of the 4-μm-thick aluminum foil for the $K\alpha$ photons ($\sim$70%) is included. This realistic pumping energy, 100 μJ/5 mm, is almost two times larger than that in the calculation described above and raises the feasibility of this scheme. It was noted that, at 5 J, the subpicosecond duration pulse with a 0.1-Hz repetition rate recently became available [42], and this repetition rate can be improved to more than 10 Hz by adopting laser-diode pumping [43].

Finally, we roughly estimate the duration of the XRL pulse and the output energy of this scheme. Under the assumption of a weakly gain-saturated regime, the peak output intensity is 4×10^{11} W/cm^2 at the plasma edge with a size of 20×6 μm, and the duration (FWHM) is narrower at around 200 fs by the effect of the amplification. This leads to an output energy of 500 nJ, which is high enough for single-shot imaging of biological samples.

IV. SUMMARY

We have investigated a photo-pumping scheme where the aluminum $K\alpha$ line is used to pump the $2p^5 4d$ excited level from the $2p^6$ ground state of the neonlike zinc ions. Detailed calculations on the atomic processes and the radiation transport of the $2p^6$-$2p^5 4d$ resonance line shows that a substantial amplification gain of $\sim$100 cm^{-1} in the transition of the $2p^5 3p$-$2p^5 4d$ line at a wavelength of 3.5 nm can be generated in this scheme by pumping with a laser of only 5 J. The XRL output energy is expected to be around 500 nJ with a pulse duration of $\sim$200 fs. Therefore, this scheme will be one of the feasible water-window XRLs using a laboratory-size pumping source.

ACKNOWLEDGMENTS

The authors thank Professor A. Y. Faenov for the fruitful discussion about the spectral matching of the aluminum $K\alpha$ and the resonance line of the neonlike zinc ions and Dr. A. Sasaki for the calculation of atomic data using the HULLAC code and ion abundance using the HYADES code. The present work was performed partly under the Joint-Research Program entitled "Quantum Beam Science by Petawatt Lasers" by The Ministry of Education, Culture, Sports and Science (MEXT) and the "Japan Basic Research Foundation (KIBAN B) Grant No. 2136052" of The Japanese Society for the Promotion of Science (JSPS).

[1] M. P. Kalachnikov *et al.*, Phys. Rev. A **57**, 4778 (1998).
[2] J. Dunn, A. L. Osterheld, R. Shepherd, W. E. White, V. N. Shlyaptsev, and R. E. Stewart, Phys. Rev. Lett. **80**, 2825 (1998).
[3] T. Kawachi *et al.*, Phys. Rev. A **66**, 033815 (2002).
[4] B. M. Luther, Y. Wang, M. A. Larotonda, D. Alessi, M. Berrill, M. C. Marconi, and J. J. Rocca, Opt. Lett. **30**, 165 (2005).
[5] T. Kawachi, A. Sasaki, M. Tanaka, M. Kishimoto, N. Hasegawa, K. Nagashima, M. Koike, H. Daido, and Y. Kato, Phys. Rev. A **69**, 033805 (2004).
[6] L. B. DaSilva *et al.*, Science **258**, 269 (1992).
[7] J. Nilsen *et al.*, Phys. Rev. A **50**, 2143 (1994).
[8] D. Kim, S. H. Son, J. H. Kim, C. Toth, and C. P. J. Barty, Phys. Rev. A **63**, 023806 (2001).
[9] S. J. Moon and D. C. Eder, Phys. Rev. A **57**, 1391 (1998).
[10] K. Moribayashi, A. Sasaki, and T. Tajima, Phys. Rev. A **58**, 2007 (1998).
[11] N. Nakano and H. Kuroda, Phys. Rev. A **35**, 4719 (1987).
[12] J. C. Gauthier, J. P. Geindre, P. Monier and C. Chenais-Popovics, J. Phys. Colloques **47**, 259 (1986).
[13] P. Monier, C. Chenais-Popovics, J. P. Geindre, and J. C. Gauthier, Phys. Rev. A **38**, 2508 (1988).
[14] K. Gabel, C. Bergmann, E. Fill, E. Forster, and I. Ushmann, Appl. Phys. B: Lasers Opt. **56**, 3 (1993).
[15] D. L. Matthews, P. Hagelstein, E. Campbell, A. Toor, R. Kauffman, L. Koppel, W. Halsey, D. Phillion, and R. Price, IEEE J. Quantum Electron. **19**, 1786 (1983).
[16] P. L. Hagelstein, Plasma Phys. **25**, 1345 (1983).
[17] J. L. Porter, R. B. Spielman, M. K. Matzen, E. J. McGuire, L. E. Ruggles, M. F. Vargas, J. P. Apruzese, R. W. Clark, and J. Davis, Phys. Rev. Lett. **68**, 796 (1992).
[18] K. J. Ilcisin, F. Aumayr, J. L. Schwob, and S. Suckewer, J. Opt. Soc. Am. B **11**, 1436 (1994).
[19] A. Y. Faenov, B. A. Bryunetkin, V. M. Dyakin, T. A. Pikuz, I. Y. Skobelev, S. A. Pikuz, J. Nilsen, A. L. Osterheld, and U. I. Safronova, Phys. Rev. A **52**, 3644 (1995).
[20] A. Vinogradov, I. Sobel'man, and E. Yukov, Sov. J. Quantum Electron. **5**, 59 (1975).
[21] U. Feldman, E. O. Hulburt and J. Reader, J. Opt. Soc. Am. B **6**, 264 (1989).

[22] M. A. Duguary and P. M. Rentzepis, Appl. Phys. Lett. **10**, 350 (1967).
[23] E. J. McGuire, Phys. Rev. Lett. **35**, 844 (1975).
[24] S. Meyer, T. Menzel, B. Wellegehausen, P.-X. Lu, S. Insam, and E. Fill, in *Proceedings of X-ray Lasers 1996*, edited by S. Svanberg (Institute of Physics, Bristol, 1997), p. 173.
[25] C. P. J. Barty, G. Y. Yin, J. E. Field, S. J. Benerofe, J. F. Young, and S. E. Harris, in *Proceedings of X-ray Lasers 1990*, edited by G. J. Tallents (Institute of Physics, Bristol, 1991), p. 21.
[26] J. Nilsen and N. Rohringer, in *Proceedings of SPIE, X-ray Lasers and Coherent X-ray Sources IX*, edited by J. Dunn and A. Klisnick (SPIE, Bellingham, 2011), 814003.
[27] P. Emma *et al.*, Nature Photon. **4**, 641 (2010).
[28] See current events in J. Synchrotron Rad. **18**, 686 (2011).
[29] J. Nilsen, in *Proceedings of SPIE, Soft X-ray Lasers and Applications VIII*, edited by G. J. Tallents and J. Dunn (SPIE, Bellingham, 2009), 74510N.
[30] M. J. Seaton, J. Phys. B **20**, 6363 (1987).
[31] B. A. Remington, R. P. Drake, H. Takabe, and D. Arnett, Phys. Plasmas **7**, 1641 (2000).
[32] A. Rousse, P. Audebert, J. P. Geindre, F. Falliès, J. C. Gauthier, A. Mysyrowicz, G. Grillon, and A. Antonetti, Phys. Rev E **50**, 2200 (1994).
[33] D. Salzmann, C. Reich, I. Uschmann, E. Forster, and P. Gibbon, Phys. Rev. E **65**, 036402 (2002).
[34] NIST Atomic Spectra Database [http://physics.nist.gov/PhysRefData/ASD/levels_form.html].
[35] E. Kallne and T. Aberg, X-Ray Spectrom. **4**, 26 (1975).
[36] V. A. Boiko, A. Y. Faenov, and S. A. Pikuz, J. Quant. Spectrosc. Radiat. Transf. **19**, 11 (1978).
[37] K. B. Fournier *et al.*, J. Quant. Spectrosc. Radiat. Transf. **81**, 167 (2003).
[38] M. Klapisch and A. Bar-Shalom, J. Quant. Spectrosc. Radiat. Transf. **58**, 687 (1997).
[39] D. H. Sampson and H. L. Zhang, Astrophys. J. **335**, 516 (1988).
[40] G. D. Davis, P. E. Viljoen, and M. G. Lagally, J. Electron Spectrosc. Relat. Phenom. **20**, 305 (1980).
[41] J. T. Larsen and S. M. Lane, J. Quant. Spectrosc. Radiat. Transf. **51**, 179 (1994).
[42] Y. Ochi, N. Hasegawa, T. Kawachi, and K. Nagashima, Appl. Opt. **46**, 1500 (2007).
[43] F. J. Furch, B. A. Reagan, B. M. Luther, A. H. Curtis, S. P. Meehan, and J. J. Rocca, Opt. Lett. **34**, 3352 (2009).